JACC: BASIC TO TRANSLATIONAL SCIENCE VOL. 4, NO. 3, 2019

PRECLINICAL RESEARCH

Western Diet-Fed, Aortic-Banded Ossabaw Swine

A Preclinical Model of Cardio-Metabolic Heart Failure

T. Dylan Olver, PhD,[a,*] Jenna C. Edwards, BS,[a,*] Thomas J. Jurrissen, BS,[b] Adam B. Veteto, MS,[c] John L. Jones, MS,[c] Chen Gao, BS,[d] Christoph Rau, PhD,[d] Chad M. Warren, MS,[e] Paula J. Klutho, PhD,[f] Linda Alex, PhD,[f] Stephanie C. Ferreira-Nichols, BS,[f] Jan R. Ivey, BS,[a] Pamela K. Thorne, MS,[a] Kerry S. McDonald, PhD,[c] Maike Krenz, MD,[c,f] Christopher P. Baines, PhD,[a,c,f] R. John Solaro, PhD,[e] Yibin Wang, PhD,[d] David A. Ford, PhD,[g] Timothy L. Domeier, PhD,[c,†] Jaume Padilla, PhD,[b,f,i,†] R. Scott Rector, PhD,[b,h,j,†] Craig A. Emter, PhD[a,†]

VISUAL ABSTRACT

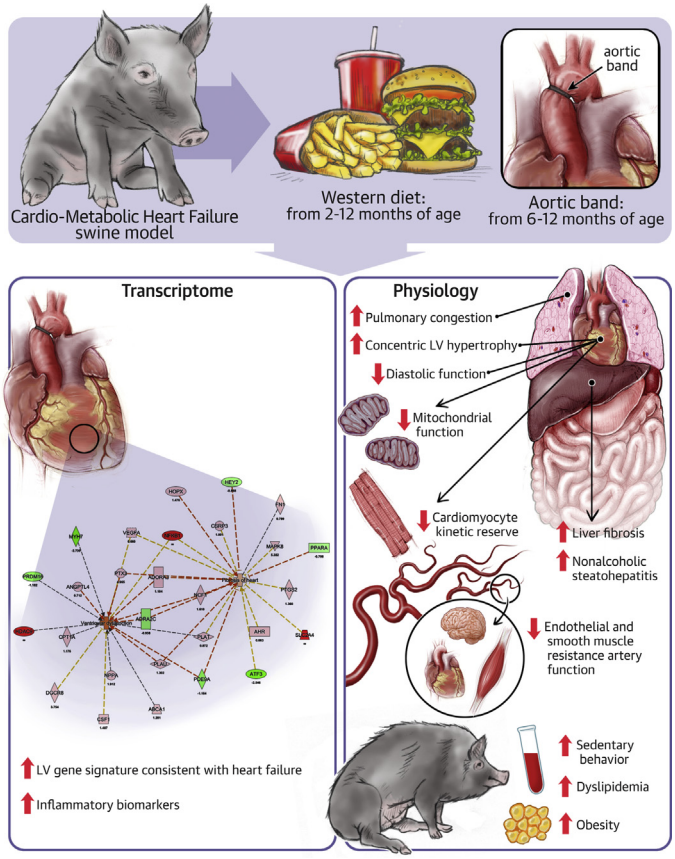

Olver, T.D. et al. J Am Coll Cardiol Basic Trans Science. 2019;4(3):404–21.

HIGHLIGHTS

- **The combination of a Western-diet and aortic banding results in a cardio-metabolic heart failure phenotype in Ossabaw swine.**
- **Ossabaw swine with cardio-metabolic heart failure display cardiac dysfunction at the whole heart and cellular levels.**
- **The left ventricle transcriptome showed gene signatures consistent with pro-inflammatory heart failure.**
- **Cardio-metabolic heart failure was coupled with microvascular dysfunction in the heart, skeletal muscle, and brain.**
- **Ossabaw swine with cardio-metabolic heart failure are sedentary and obese with liver dysfunction.**

From the [a]Department of Biomedical Science, University of Missouri-Columbia, Columbia, Missouri; [b]Department of Nutrition and Exercise Physiology, University of Missouri-Columbia, Columbia, Missouri; [c]Department of Medical Pharmacology and Physiology, University of Missouri-Columbia, Columbia, Missouri; [d]David Geffen School of Medicine, University of California, Los Angeles,

ISSN 2452-302X https://doi.org/10.1016/j.jacbts.2019.02.004

SUMMARY

The development of new treatments for heart failure lack animal models that encompass the increasingly heterogeneous disease profile of this patient population. This report provides evidence supporting the hypothesis that Western Diet–fed, aortic-banded Ossabaw swine display an integrated physiological, morphological, and genetic phenotype evocative of cardio-metabolic heart failure. This new preclinical animal model displays a distinctive constellation of findings that are conceivably useful to extending the understanding of how pre-existing cardio-metabolic syndrome can contribute to developing HF.

ABBREVIATIONS AND ACRONYMS

AB = aortic-banded
CON = control
EDPVR = end-diastolic pressure–volume relationship
EF = ejection fraction
HF = heart failure
HFpEF = heart failure with preserved ejection fraction
HFrEF = heart failure with reduced ejection fraction
IL1RL1 = interleukin 1 receptor-like 1
LV = left ventricle
NF = nuclear factor
PTX3 = pentraxin-3
WD = Western Diet

Heart failure (HF) is currently among the most challenging issues facing the treatment of cardiovascular disease. Of the approximately 6 million patients with HF in the United States, there is an approximately equal diagnosis of HF with reduced ejection fraction (HFrEF) and HF with preserved ejection fraction (HFpEF) (1-5). The disease profile of HF patients is becoming more heterogeneous, often displaying various combinations of numerous comorbidities, including obesity, metabolic syndrome, diabetes, and hypertension. Although the prevalence of HF is expected to increase during the next 15 years, traditional treatments for HF have remained largely unchanged over the last 20 years. Furthermore, HFpEF patients are largely unresponsive to standardized therapeutic approaches proven effective for HFrEF (1,2,6-9). Thus, new therapeutic targets for HF patients are desperately needed.

The development of effective treatments for HF patients may be limited by a lack of translational animal models that encompass the wide ranging pathology of an ever-increasing population of HF patients with pre-existing cardio-metabolic syndrome. Recently, attention has focused on the role of increased systemic inflammation that results from common risk factors for developing HF. This has prompted discussion regarding the need to develop preclinical animal models that include comorbidities in parallel with a HF phenotype. A number of syndromes may predispose patients to HF, including metabolic disease (e.g., obesity, insulin resistance), hypertension, renal disease, and coronary artery disease. Impairment in multiple organ systems, including both central (cardiac morphology, coronary vasculature, both systolic and diastolic function, cardiac reserve) and peripheral (pulmonary, renal, hepatic, immune, skeletal muscle, cerebral, and associated vascular beds) components, has been highlighted as a critical risk factor predisposing patients to HF. Comprehensive

Los Angeles, California; [e]Department of Physiology and Biophysics, Center for Cardiovascular Research, University of Illinois at Chicago, Chicago, Illinois; [f]Dalton Cardiovascular Research Center, University of Missouri-Columbia, Columbia, Missouri; [g]Department of Biochemistry and Molecular Biology and Center for Cardiovascular Research, Saint Louis University- School of Medicine, St. Louis, Missouri; [h]Department of Medicine - University of Missouri-Columbia, Columbia, Missouri; [i]Department of Child Health, University of Missouri-Columbia, Columbia, Missouri; and the [j]Research Service, Harry S Truman Memorial VA Hospital, University of Missouri-Columbia, Columbia, Missouri. *Dr. Oliver and Ms. Edwards contributed equally to this work and are joint first authors. †Drs. Domeier, Padilla, Rector, and Emter contributed equally to this work and are joint senior authors. This study was supported by a University of Missouri Research Board Grant (principal investigators [PIs]: Drs. Emter and Rector); National Institutes of Health (NIH) Grant RO1 HL112998 (PI: Dr. Emter); VA-Merit Grant I01BX003271-01 (PI: Dr. Rector); NIH Grant K01 HL125503 (PI: Dr. Padilla); NIH Grant K01 AG041208 and R01 HL136292 (PI: Dr. Domeier); American Heart Association postdoctoral fellowship 16POST27760052 (PI: Dr. Olver); NIH Grant R01 HL094404 (PI: Dr. Baines); NIH Grant R01 GM115552 (PI: Dr. Ford); NIH Grants R01 HL122737, NIH R01 HL123295, and NIH HL129639 (PI: Dr. Wang); American Heart Association postdoctoral fellowship 17POST33661136 (PI: Dr. Gao); NIH Grant R01 HL116525 (PI: Krenz); and NIH Grant PO1 HL62426 (Project 1, Dr. Solaro; Core C: Dr. Warren). The authors acknowledge NIH grants RR013223 and HL062552 to M. Sturek and the CMP of IUSM and Purdue University, and NIH grant U42 OD011140 to R. Prather and the National Swine Resource and Research Center at the University of Missouri-Columbia for the Ossabaw swine. Dr. Solaro has served on the Scientific Advisory Board and been a consultant for Cytokinetics; and has a fee-for-service agreement with Pfizer. Dr. Wang has been a consultant for REMD Biotherapeutics. All other authors have reported that they have no relationships relevant to the contents of this paper to disclose. All authors attest they are in compliance with human studies committees and animal welfare regulations of the authors' institutions and Food and Drug Administration guidelines, including patient consent where appropriate. For more information, visit the *JACC: Basic to Translational Science* author instructions page.

Manuscript received January 17, 2019; revised manuscript received February 13, 2019, accepted February 21, 2019.

TABLE 1 Postmortem Analysis of Heart and Lung Morphology, and Pressure–Volume Assessment of Resting Systolic and Diastolic LV Function

Gross Morphology	CON (n = 5)	WD-AB (n = 5)	*t*-Test (p Value)
Body surface area (m^2)	1.10 ± 0.01	1.51 ± 0.04*	<0.0001
Tibia length (cm)	16.6 ± 0.2	16.6 ± 0.1	0.93
Lung weight (g)	236 ± 11	294 ± 12†	0.01
Heart weight (g)	157 ± 4	229 ± 6*	<0.0001
LV+S weight (g)	107 ± 2	150 ± 4*	<0.0001
RV weight (g)	28 ± 2	46 ± 2‡	<0.001
Atria weight (g)	21 ± 2	33 ± 1‡	<0.001
LV Function: Pressure-Volume and Echocardiography	**CON (n = 4 to 5)**	**WD-AB (n = 4 to 5)**	***t*-Test (p Value)**
Systolic function			
HR (beats/min)	94 ± 17	80 ± 8	0.49
LVESV (ml)	48 ± 6	33 ± 9	0.21
LVESP (mm Hg)	94 ± 12	102 ± 6	0.54
LVEF (%)	52 ± 3	63 ± 5	0.12
LV SV (ml)	50 ± 2	51 ± 5	0.83
LV SVI (ml/m^2)	46 ± 1	34 ± 4§	<0.05
ESPVR (mm Hg/ml)	11 ± 5	23 ± 7	0.21
PRSW (mm Hg)	65 ± 10	91 ± 8	0.09
Diastolic function			
LVEDV (ml)	98 ± 6	84 ± 12	0.34
LVEDP (mm Hg)	10 ± 1	8 ± 2	0.22
EDPVR (mm Hg/ml)	0.015 ± 0.003	0.040 ± 0.010§	<0.05
LV untwisting: apical early diastolic rotation rate (°/s)	112 ± 6	94 ± 4§	<0.05
LV global longitudinal late diastolic strain rate (1/s)	1.1 ± 0.1	1.8 ± 0.1*	<0.0001

Values are mean ± SE. *p < 0.0001. †p < 0.01. ‡p < 0.001. §p < 0.05; for significantly different versus control (CON).

Atria = right + left atria; EDPVR = end-diastolic pressure–volume relationship; ESPVR = end-systolic pressure–volume relationship; HR = heart rate; LV = left ventricular; LVEDP = LV end-diastolic pressure; LVEDV = LV end-diastolic volume; LVEF = LV ejection fraction; LVESP = LV end-systolic pressure; LVESV = LV end-systolic volume; LV+S = LV + septum; LV SV = LV stroke volume; LV SVI = LV stroke volume index; PRSW = preload recruitable stroke work; RV = right ventricle; WD-AB = Western diet, aortic banded.

characterization of animal models of experimental HF that include multisystem contributions to the overall pathology are therefore critical to advancing the understanding of a growing population of HF patients with multiple pre-existing comorbidities.

SEE PAGE 422

A number of previous reports from our laboratory (and others) showed that Ossabaw swine, a unique translational large animal model genetically predisposed to obesity and metabolic derangement, do not develop HF from dietary intervention alone (10-17). Furthermore, our laboratory previously published numerous studies that examined the impact of aortic banding alone (in the absence of comorbidities) on developing disease in a separate preclinical swine model of HF (18-27). Thus, the primary goal of this study was to develop a swine model of experimental cardio-metabolic HF. Specifically, our aim was to determine whether the combination of dietary and pressure-overload interventions would produce a cardio-metabolic HF phenotype. We hypothesized Western Diet (WD)–fed Ossabaw swine subject to chronic cardiac pressure overload by aortic banding would display physiological, morphological, and genetic phenotypes relevant to patients with pre-existing metabolic derangement who are at risk of developing HF. We provide detailed integrated analyses that demonstrate the potential relevance of this preclinical swine model for cardio-metabolic HF (28,29).

METHODS

EXPERIMENTAL DESIGN. Two-month-old, intact female Ossabaw swine (15 to 20 kg, Ossabaw pigs were generously provided by: 1) Michael Sturek, PhD, in the Ossabaw Swine Resource, Comparative Medicine Program at Purdue University and Indiana University School of Medicine; and 2) Randall Prather, PhD, and Eric M. Walters, PhD, in the National Swine Resource and Research Center at the University of Missouri-Columbia), were assigned into 2 groups: nonsham sedentary control (CON) (n = 5) and WD-fed aortic-banded (WD-AB) with HF (n = 7). Two animals were lost in the WD-AB group as a result of not surviving the aortic banding surgery at 6 months of age; both animals weighed >50 kg at the time of surgery. We believe this issue can be remedied through weight control in the initial phases of obesity development, given all WD-AB animals in the current study under this specific weight threshold survived without surgical complications following thoracotomy. A third animal was lost to sudden cardiac death 1 week before terminal experiments were scheduled in the WD-AB group. Necrospy of this animal revealed complications due to renal infarction, pulmonary and hepatic congestion, and a systemic inflammatory process. Ultimately, outcome measures in the WD-AB group were assessed in 4 to 5 animals.

The CON group ingested a standard chow diet (5L80, Lab Diet; 3.03 $kcal/g^{-1}$; carbohydrate: 71%; protein: 18.5%, and fat: 10.5%; 500 g/day), whereas the WD-AB group was fed a WD (1,000 g/day) high in fat, high-fructose corn syrup, and cholesterol (5B4L, Laboratory Diet; 4.14 $kcal/g^{-1}$; carbohydrate: 40.8% [17.8% of total calories from high-fructose corn syrup]; protein: 16.2%; fat: 43%, 2% cholesterol wt/wt) as previously reported (13-17). At 6 months of age, aortic banding was used to induce HF as previously described (19-23,25-27). A trans-stenotic systolic gradient of approximately 70 mm Hg (72 ± 2 mm Hg) was achieved under anesthesia using phenylephrine (intravenously 1 to 3 μg/kg/min) to maintain a distal

TABLE 2 Serial Echocardiographic Assessment of LV Morphology

	CON (n = 5)			WD-AB (n = 5)			
	Age 6 months	Age 8 months	Age 12 months	Pre-AB Age 6 months	Post-AB Age 8 months	Post-AB Age 12 months	RM ANOVA
Body weight (kg)	31 ± 2	36 ± 2	46 ± 1†††	45 ± 2***	56 ± 3***†††	76 ± 3***†††	ME group##
LVIDd (mm)	40 ± 1	41 ± 1	45 ± 1†	37 ± 1	42 ± 1†	46 ± 2††	ME time##
LVIDs (mm)	24 ± 1	25 ± 1	26 ± 1	23 ± 1	21 ± 1	23 ± 2	p = 0.33
LV WTd (mm)	6.2 ± 0.5	6.4 ± 0.2	5.7 ± 0.3	6.6 ± 0.2	9.8 ± 0.3***††	9.7 ± 0.5***††	Interaction‡
LV WTs (mm)	10.0 ± 0.5	11.0 ± 0.3	11.3 ± 0.4	11.8 ± 0.3**	14.8 ± 0.3***††	16.1 ± 0.4***††	Interaction§

Values are mean ± SE. Statistics: Post hoc versus CON at the same time point (**p < 0.01; ***p < 0.001); main effect (ME) (##p < 0.0001); interaction effect = group × time (§ p <0.01, ‡p < 0.001); †post hoc within same group versus 6-month time point (†p < 0.01; †† p < 0.001; p < 0.0001).

LVIDd = left ventricular internal diastolic dimension; LVIDs = left ventricular internal systolic dimension; LV WTd = left ventricular diastolic wall thickness; LV WTs = left ventricular systolic wall thickness; RM ANOVA, repeated measure analysis of variance.

peripheral vascular mean aortic pressure of approximately 90 mm Hg (87 ± 2 mm Hg) at a heart rate of 85 beats/min (84 ± 3 beats/min). In total, Ossabaw swine in the WD-AB group were subjected to 10 months of WD and 6 months of chronic cardiac pressure overload. Body surface area was calculated as previously published for swine (30,31). Animals were fed once per day, and water was provided ad libitum. All animal protocols were in accordance with the Principles for the Utilization and Care of Vertebrate Animals Used in Testing Research and Training and approved by the University of Missouri Animal Care and Use Committee.

STATISTICAL ANALYSIS. Data analyses were performed using SPSS (version 19.0, IBM, Armonk, New York) or SigmaStat (version 3.5, Systat Software, San Diego, California). Linear regression was used to examine the relationship between inflammatory biomarkers and diastolic function. Group comparisons were made using a Student's *t*-test (32). Group comparisons for in vitro vascular function and serial ultrasound morphological experiments were made using a repeated-measures analysis of variance (group × dose and group × time, respectively). Group differences revealed by analysis of variance were found using Student Newman-Keuls post hoc analysis. Interobserver variability for ultrasound measures was evaluated using the intraclass correlation coefficient in a 2-way random model (<0.40: poor agreement; 0.40 to 0.75: good agreement; >0.75: excellent agreement) (33). Power analyses were conducted to determine the appropriate number of pigs to detect differences between groups as recommended by Kim and Seo (34) using the Sealed Envelope Power Calculator (https://www.sealedenvelope.com/power/continuous-superiority). For input, we used published end-diastolic pressure–volume relationship (EDPVR) data reported in 6 CON and 7 AB pigs (20) because of the well-established development of diastolic dysfunction in patients with metabolic syndrome and the reputation of EDPVR as a gold standard for measuring diastolic function. Significance level was set to 5%, power to 80%, mean outcome in control group = 0.011, mean outcome in experimental group = 0.021, and standard deviation = 0.004 (20). This power analysis indicated 4 swine per group would be sufficient. All data are presented

TABLE 3 Ingenuity Pathway and Gene Ontology Analyses of Induced Heart Failure-Related Gene Pathways Expressed between CON and WD-AB Left Ventricle

Ingenuity Pathway Analysis, Top Toxicology Lists		
Name		**p Value**
Cardiac hypertrophy		<0.0001
Increases renal damage		<0.0001
Renal necrosis/cell death		<0.0001
Cardiac fibrosis		<0.0001
Liver proliferation		<0.0001
Name	**Matched Gene Symbols**	**p Value**
Gene ontology, signaling pathways: heart failure		
Cardiomyocyte differentiation through BMP receptors	MYH7, MYH7B, NPPA, NPPB, BMP4, BMP5	<0.0001
Hypertrophy model	EIF4E, IL1R1, IFRD1, ATF3, VEGFA	<0.001
Gene ontology, function-based analysis phenotype: heart failure		
Cardiac fibrosis	ACKR3, AHR, HEY2, PPARA, HOPX, PTGS2, THBS4, CSRP3, MAPK8, PDL	<0.001
Gene ontology, diseases: heart failure		
Myocardial infarction	ABCA1, ALDH2, CCL2, CIITA, F13A1, HMGCR, LDLR, NPPA, NPPB, PLAT, PROCR, PTGS2, SELP, THBS4, TLR4, TNNT1, VEGFA	<0.0001
Dilated cardiomyopathy	ADRA2C, ANKRD2, CCL2, CSRP3, KCNIP2, LAMA2, MYH7, NPPA, NPPB, PDLIM3, PGM1, SUN2, TNNI1, TNNT1, VCAM1	<0.0001
Pulmonary fibrosis	CCL2, CD24, CTGF, CXCL8, MMP11, RGS1, SLN, UBD, VCAM1	<0.01
Left ventricular noncompaction	CSRP3, MYH7, MYH7B, PRDM16, YWHAE	<0.01
Pulmonary hypertension	ADORA3, BMP4, NPPA, NPPB, PDE4A, PLAT, VEGFA	<0.01
Heart disease	C3, HMGCR, MYH7, NPPA, NPPB, PPARA	<0.05
Atrial fibrillation	NPPA, NPPB, PLAT, SCN3B, SELP	<0.05
Hypertrophic cardiomyopathy	CSRP3, MYH7, NPPB, TNNT1	<0.05

BMP = bone morphogenic protein; other abbreviations as in Table 1.

FIGURE 1 Representative P-V Loops

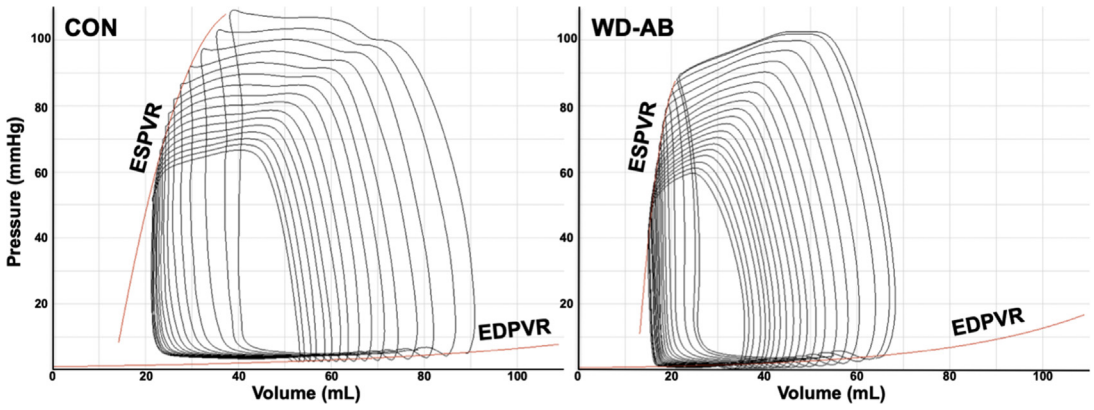

Representative pressure–volume (P-V) loops at rest from individual control (CON) and Western diet, aortic-banded (WD-AB) animals. EDPVR = end-diastolic P-V relationship; ESPVR = end-systolic P-V relationship.

as means ± SE, and significance was reported at $p < 0.10$ and $p < 0.05$ levels (35,36).

See Supplemental Material for a comprehensive account of all Methods utilized in the current study (Supplemental Tables 1 to 3, Supplemental Figures 1 to 8, and Supplemental References).

RESULTS

CARDIAC REMODELING AND FUNCTION. **Tables 1 to 3 and Figures 1 to 4** provide evidence supporting functional, structural, and genetic characteristics consistent with HF in the WD-AB group using echocardiographic, pressure–volume, post-mortem morphology, and RNA-seq techniques. Considering 1 independent variable was diet, tibia length was examined to determine if normalization of the morphometric data was necessary (37,38). Tibia length was the same between groups, indicating that differences in body weight and body surface area between groups were observed in animals with similar age-related growth (**Table 1**). Because there were no significant differences in tibia length, absolute heart and lung weights were used for group morphological analyses (39). WD-AB animals displayed increased lung weight compared with the CON group, with no differences in resting ejection fraction (EF) (**Table 1**). Significant concentric left ventricular (LV) hypertrophy was present in WD-AB animals, as indicated by an increase in global hypertrophy (LV, right ventricle, and atria) (**Table 1**) and increased LV diastolic wall thickness 2 and 6 months post-aortic banding that was dependent on the group at 8 and 12 months of age, respectively (**Table 2**) (group × time interaction; representative ultrasound images are shown in Supplemental Figures 1A and 1B). There were no differences in LV internal diastolic dimension or end-diastolic volume between groups (**Tables 1 and 2**). Analysis of aortic hemodynamics (proximal to the AB in the WD-AB group) (Supplemental Table 1) indicated WD-AB animals faced a greater afterload compared with CON animals, which was evident 6 months post-aortic banding as significant increases in both aortic systolic blood pressure and pulse pressure.

Additional analysis of LV function resulted in paradoxical findings with respect to systolic function. Stroke volume (**Table 1**) and torsion (Supplemental Figure 1D) relative to cardiac remodeling were similar between groups. There was a trend toward increased LV contractility (measured as preload recruitable stroke work, shown by our laboratory and others in AB swine) (20,23,24,40) in the WD-AB group, which was observed in parallel with a decreased stroke volume index (**Table 1**). **Figure 2** outlines the potential contributions of individual cardiomyocyte function to whole heart cardiac dysfunction (representative traces of calcium transients and sarcomere length are presented in Supplemental Figures 2A and 2B). Diastolic and systolic calcium and sarcomere length (Supplemental Figures 2C and 2D), as well as calcium transient and shortening amplitudes (Supplemental Figures 2E and 2F), were comparable between the CON and WD-AB groups under both baseline and dobutamine (1 μM) experimental conditions, which was consistent with preserved systolic function at the whole organ level. However, differences among groups were apparent in

FIGURE 2 **Ossabaw Swine Fed A WD With Chronic Pressure Overload-Induced HF Show Impaired Individual Cardiomyocyte Function**

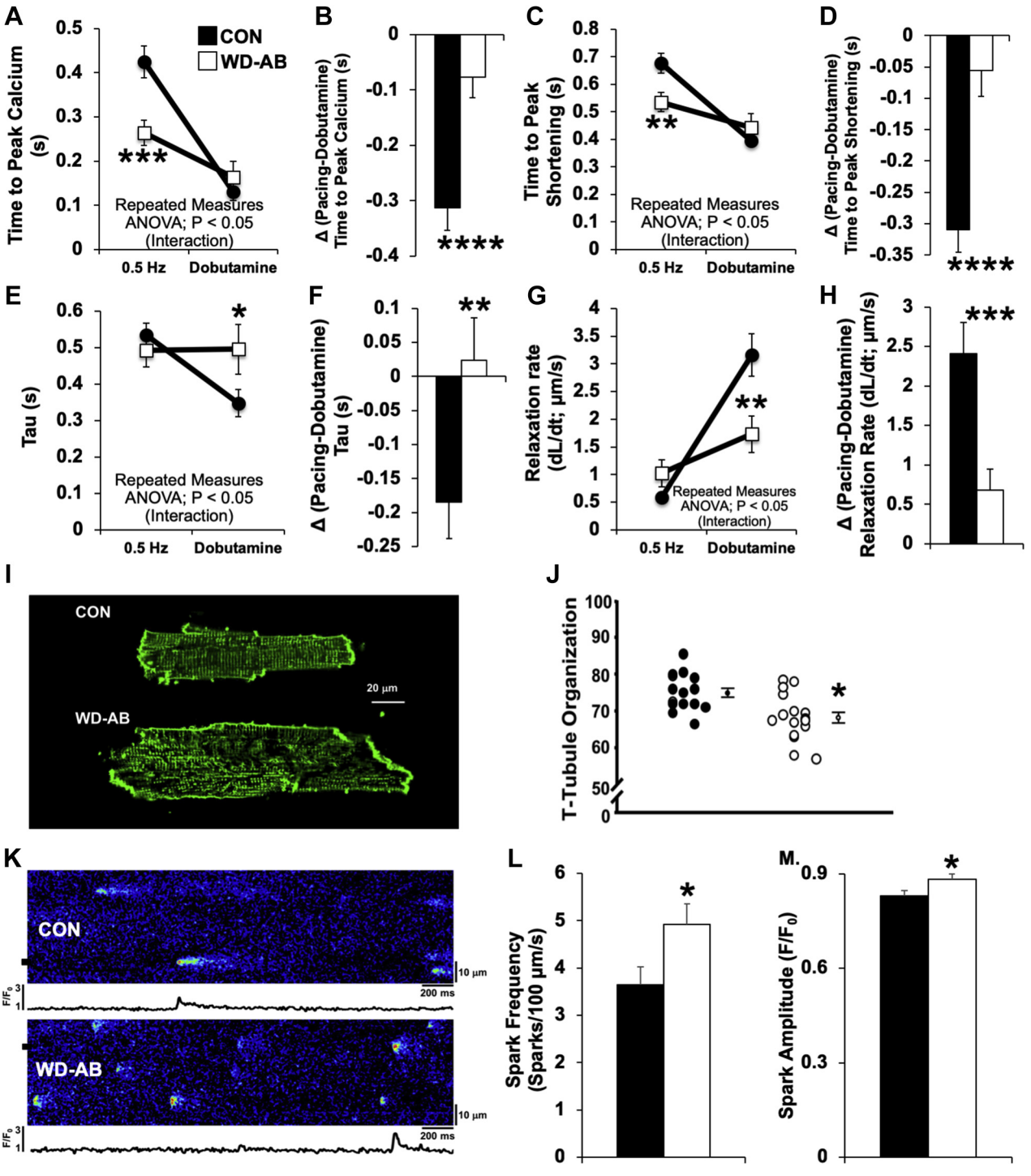

(A) Systolic cardiomyocyte calcium and **(C)** shortening kinetics are faster under baseline pacing conditions in the WD-AB group, but **(B and D)** lack β-adrenergic reserve in response to dobutamine. **(E and F)** Diastolic calcium reuptake (tau) and **(G and H)** relaxation rate kinetic reserve following exposure to dobutamine is impaired in WD-AB cardiomyocytes. **(I)** Representative cardiomyocyte images show **(J)** cardiomyocyte t-tubule disorganization in WD-AB animals. **(K)** Representative line scans illustrate spontaneous ryanodine receptor-mediated calcium **(L)** spark frequency and **(M)** amplitude were increased in the WD-AB group. *t-test versus CON (*$p < 0.05$; **$p < 0.01$; ***$p < 0.001$; ****$p < 0.0001$). n = 4 animals, 25 to 27 cells in the CON group; n = 4 animals, 23 to 25 cells in the WD-AB group. ANOVA = analysis of variance; HF = heart failure; other abbreviations as in Figure 1.

FIGURE 3 Isolated Mitochondrial Function Is Compromised in Ossabaw Swine Fed a WD With Chronic Pressure Overload-Induced HF and Associated With Decreased L_4CL

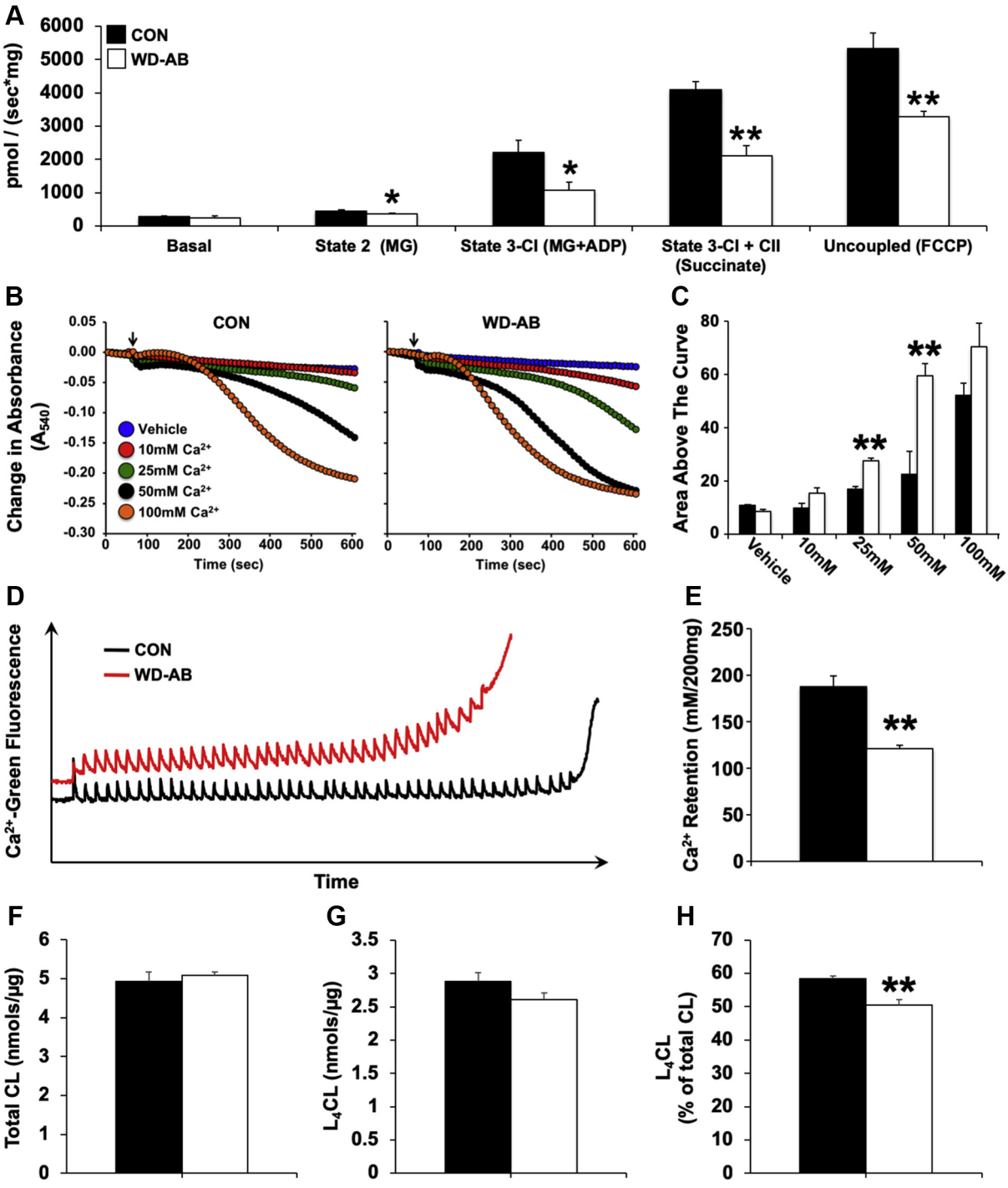

(A) Mitochondrial dysfunction evident as impaired complex 1 and 2-dependent respiration and functional uncoupling of the respiratory chain and adenosine triphosphate synthesis. **(B to E)** Susceptibility to calcium (Ca^{2+})-induced mitochondrial permeability transition (an early indicator of mitochondrial dysfunction) was increased in the WD-AB group. **(B and C)** Quantification of the area above the curve of the Ca^{2+}-induced swelling traces was increased in WD-AB animals. **(D and E)** Conversely, Ca^{2+}-retention capacity was decreased in the WD-AB group. **(F to H)** The composition of **(G)** tetralinoleoyl cardiolipin (L_4CL) to **(F)** total cardiolipin levels was **(H)** decreased in WD-AB animals. *t-test versus CON (*$p < 0.05$; ** $p < 0.01$). $n = 4$ for CON and WD-AB groups. ADP = adenosine diphosphate; MG = malate/glutamate; other abbreviations as in Figures 1 and 2.

FIGURE 4 Ossabaw Swine Fed a WD With Chronic Pressure Overload-Induced HF Exhibit Distinct Molecular Signatures Indicative of LV Pathological Remodeling

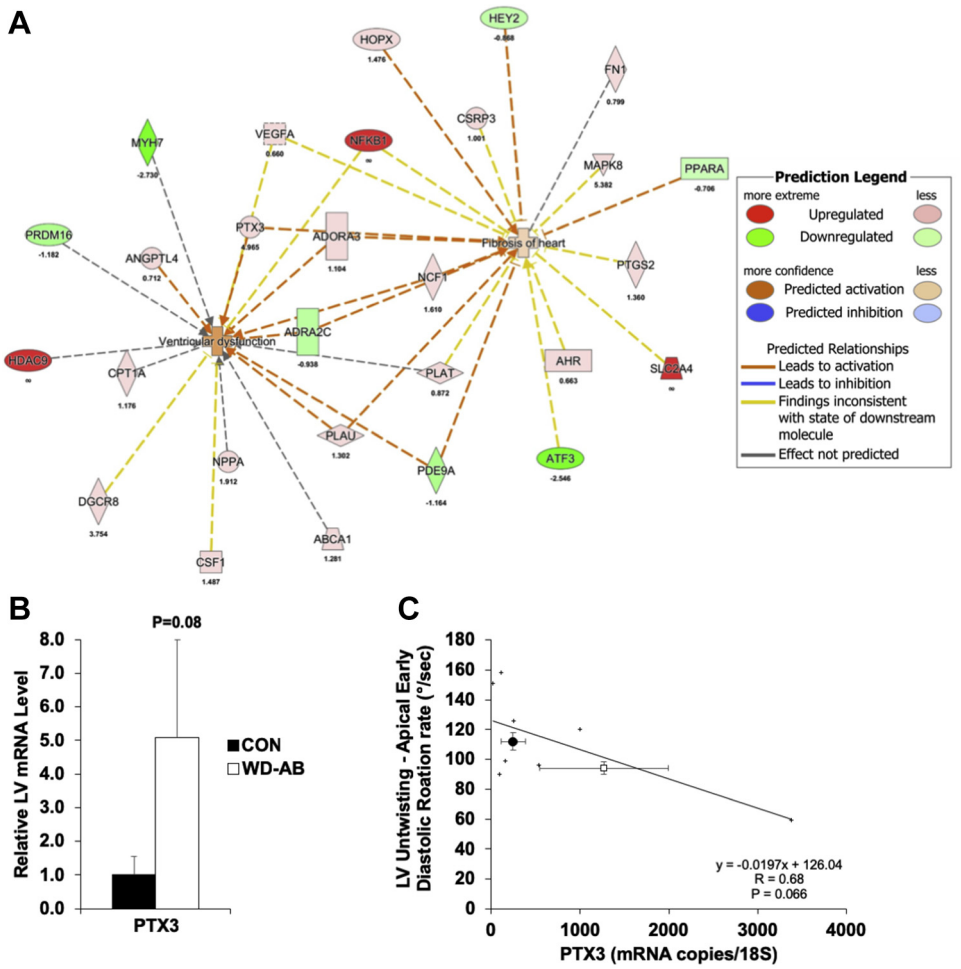

(A) Left ventricular (LV) gene interactions between significant cardiac hypertrophy and cardiac fibrosis networks revealed by ingenuity pathway analysis between CON and WD-AB animals. **(B)** Pentraxin-3 (PTX3) mRNA level is increased in the WD-AB group and **(C)** negatively correlated with LV untwisting. WD-AB animals show a right and downward shift along this relationship compared with CON (+ = individual animal data points forming the regression line). **(D)** Interleukin 1 receptor-like 1 (IL1RL1) mRNA level was also increased in the WD-AB group and **(E)** negatively correlated with LV untwisting. WD-AB animals again show a right and downward shift along this relationship compared with CON (+ = individual animal data points forming the regression line). **(F)** The collagen I/III mRNA ratio is increased in the WD-AB group. **(G)** A decrease in the more compliant N2BA titin isoform is seen in WD-AB animals with representative samples from both the CON and WD-AB groups presented alongside the bar graph. *t-test versus CON ($*p < 0.05$). n = 3 for CON and WD-AB in Figure 4A. n = 5 for the CON group and n = 4 for the WD-AB group in Figures 4B to 4G. Abbreviations as in Figures 1 and 2.

Continued on the next page

calcium transient and shortening kinetics, which resulted in a loss in dobutamine-induced functional kinetic reserve (Figures 2A to 2D). Decreases in cardiomyocyte time to peak calcium (Figures 2A and 2B) and shortening (Figures 2C and 2D) following dobutamine challenge were blunted in the WD-AB group compared with the CON group, despite showing faster cellular systolic kinetics under 0.5-Hz baseline pacing conditions. These combined data suggest that although traditional indicators of systolic function like EF appear normal, the means by which resting systolic function is maintained is substantially different in WD-AB animals.

Diastolic function was also impaired in both the whole heart and individual cardiomyocytes in WD-AB animals. The EDPVR was increased in the WD-AB

FIGURE 4 Continued

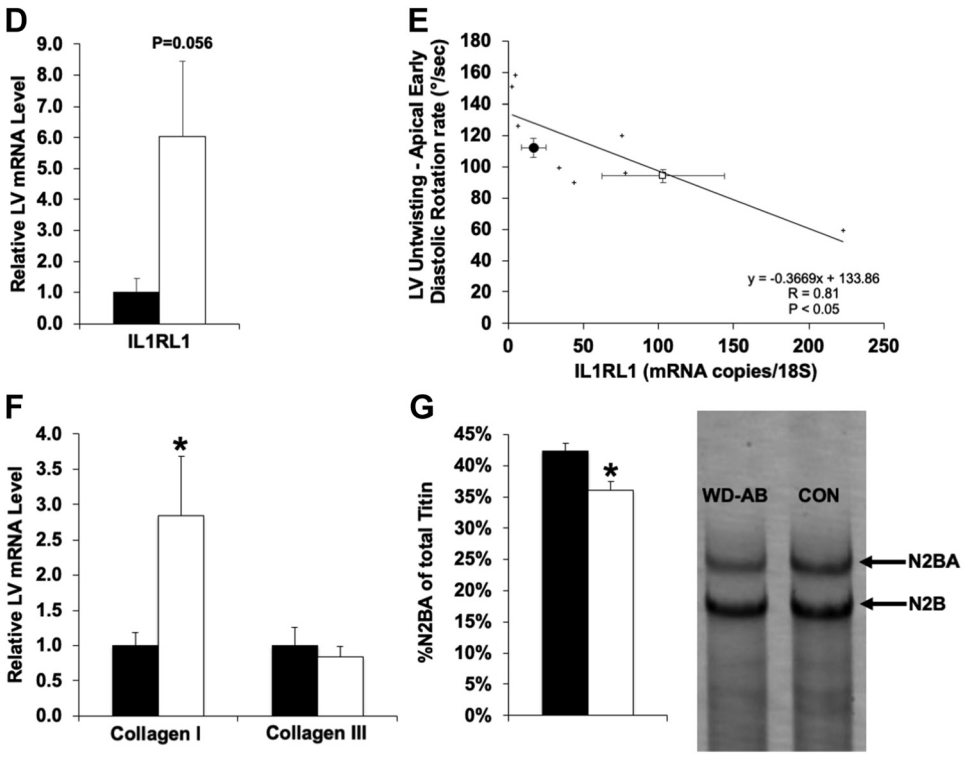

group (representative pressure–volume loops are shown in Figure 1, and quantification is shown in Table 1). This was observed in parallel with abnormal LV diastolic mechanics, including decreased LV early diastolic untwisting and increased LV late longitudinal strain rate, which were indicative of both impaired early diastolic filling and enhanced atrial systole during late diastole, respectively (Table 1). At the cellular level, dobutamine-induced enhancement in diastolic kinetic parameters, including calcium reuptake rate (Figures 2E and 2F) (tau) and relaxation rate (Figures 2G and 2H), were lost in the WD-AB group, although baseline (0.5 Hz) values were similar between groups. In addition, cardiomyocyte t-tubules were disorganized (Figures 2I and 2J), and spontaneous ryanodine receptor–mediated calcium spark frequency and amplitude were increased (Figures 2K and 2L) in WD-AB animals versus CON animals. In total, these data indicate functional and structural changes at the organ and cellular levels consistent with diastolic dysfunction.

Impaired myocardial relaxation might also have been influenced by metabolic derangement in the LV. Figure 3 shows LV mitochondrial dysfunction, including decreased complex 1- and 2-dependent respiration and *t*rifluoromethoxy carbonylcyanide phenylhydrazone (FCCP)-uncoupled maximal mitochondrial respiration (Figure 3A). Calcium-induced mitochondrial swelling was exacerbated (Figures 3B and 3C), and calcium retention capacity (Figures 3D and 3E) was also decreased in WD-AB animals, which both indicated increased susceptibility to calcium-induced mitochondrial permeability transition. Shotgun lipidomic showed the proportion of contribution of tetralinoleoyl cardiolipin to total myocardial cardiolipin levels (Figures 3F to 3H) (a phospholipid that consists of ~80% of ventricular cardiolipin in humans and is considered to reflect a healthy phospholipid phenotype in the heart) (41) was decreased in the WD-AB group. Collectively, evidence of impaired LV mitochondrial energetics is consistent with the development of HF (42).

To define the molecular signature associated with the pathological state in the WD-AB heart, transcriptome was profiled in LV tissues from WD-AB and CON animals. As presented in Table 3 and Figure 4, unbiased Ingenuity Pathway Analysis detected top gene expression changes in the WD-AB group are cardiac hypertrophy and cardiac fibrosis, which are listed as the #1 and #4 top significant toxicology lists

FIGURE 5 Ossabaw Swine Fed a WD With Chronic Pressure Overload-Induced HF Demonstrate Skeletal Muscle and Brain Vascular Dysfunction in Isolated Microvessels

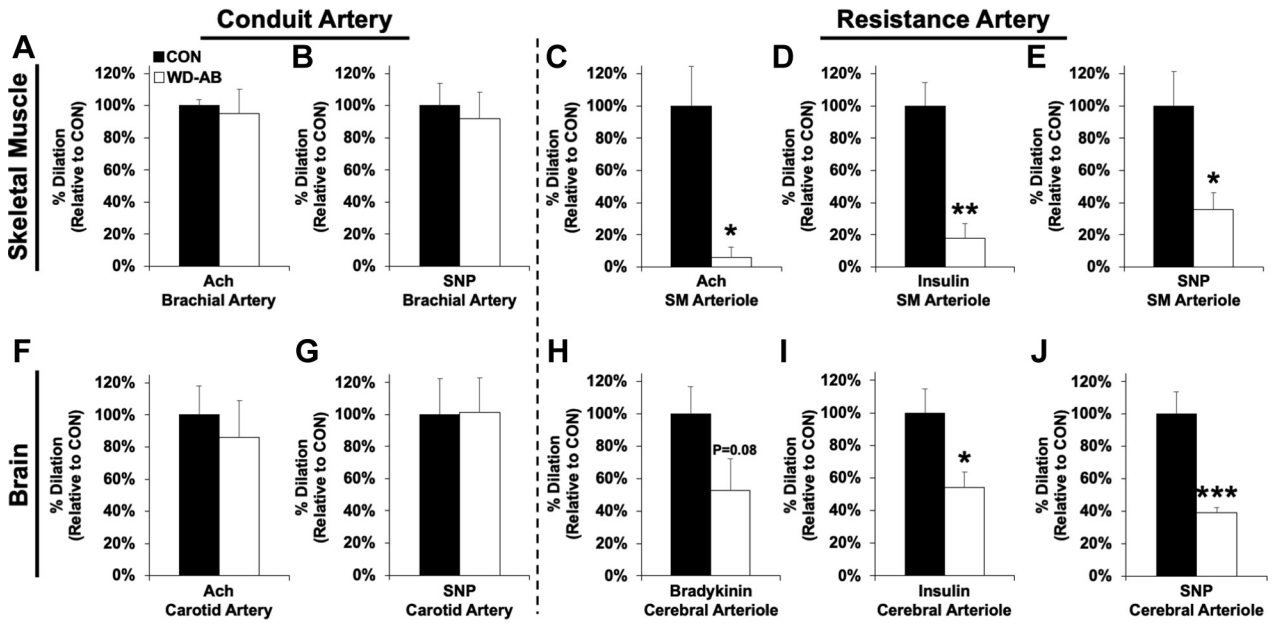

Brachial artery ring preparations indicate **(A)** endothelial and **(B)** smooth muscle–dependent function is similar between the CON and WD-AB groups. Skeletal muscle microvessel preparations show significant **(C)** endothelial, **(D)** metabolic, and **(E)** smooth muscle–dependent dysfunction in the WD-AB group. Carotid artery ring preparations reveal **(F)** endothelial and **(G)** smooth muscle–dependent function is similar between the CON and WD-AB group. Cerebral microvessel preparations show significant **(H)** endothelial, **(I)** metabolic, and **(J)** smooth muscle–dependent dysfunction in WD-AB animals. *t-test versus CON (*$p < 0.05$; **$p < 0.01$; ***$p < 0.001$). n = 5 for the CON group, and n = 4 for the WD-AB group. Ach = acetylcholine; SM = skeletal muscle; SNP = sodium nitroprusside; other abbreviations as in Figures 1 and 2.

(Table 3). Significant interaction between gene networks associated with cardiac dysfunction and fibrosis are also identified and illustrated in Figure 4A. Based on gene ontology analysis for the differentially expressed genes, a significant enrichment of several HF-related gene networks was found in the WD-AB hearts, as highlighted by numerous genes known to be implicated in HF-related cardiac fibrosis and hypertrophic remodeling, such as *NPPA*, *NPPB*, *MYH7*, as well as bone morphogenic proteins and collagens (Table 3). In addition to these well-known molecular markers for HF, a number of inflammatory genes were also implicated, including pentraxin-3 (PTX3) (43,44) and interleukin 1 receptor-like 1 (IL1RL1) (44,45), which are indicators of inflammation. The approximate 5-fold increase in PTX3 reported by RNA-seq in WD-AB animals was confirmed independently using quantitative real-time polymerase chain reaction (Figure 4B), as was an increase in IL1RL1 (Figure 4D). Cumulative group data, represented by the regression line, also showed a significant negative correlation between LV untwisting and both PTX3 (Figure 4C) and IL1RL1 (Figure 4E) mRNA levels. Group means reflected a right and downward shift along this relationship in the WD-AB group compared with the CON group, which indicated that an increase in LV expression of these markers of inflammation was associated with a decline in LV diastolic mechanical function. Cardiac remodeling in the WD-AB group was confirmed separately by 2 different measures that could influence the stiffness of individual cardiomyocytes and/or the whole heart: 1) an increase in the collagen I/III mRNA ratio (Figure 4F) (indicative of potentially increased extracellular matrix stiffness) (46); and 2) a decrease in protein expression of the N2BA isoform of titin (Figure 4G) (a more compliant isoform of the large elastic sarcomeric protein) (47-51). Total LV collagen protein was the same between the groups and visualized by representative Masson's trichrome images (Supplemental Figure 3). This suggested that differences in LV stiffness regulated by the extracellular matrix might be more related to changes in its composition (i.e., collagen isoform shift) as opposed to a general accumulation of total fibrotic components. Overall, these data are indicative of molecular signatures consistent with cardio-metabolic disease in the myocardium of WD-AB animals and suggest

FIGURE 6 Ossabaw Swine Fed a WD With Chronic Pressure Overload-Induced HF Exhibit a Systemic Inflammatory State Consistent With Common Comorbidities Seen in Experimental HF

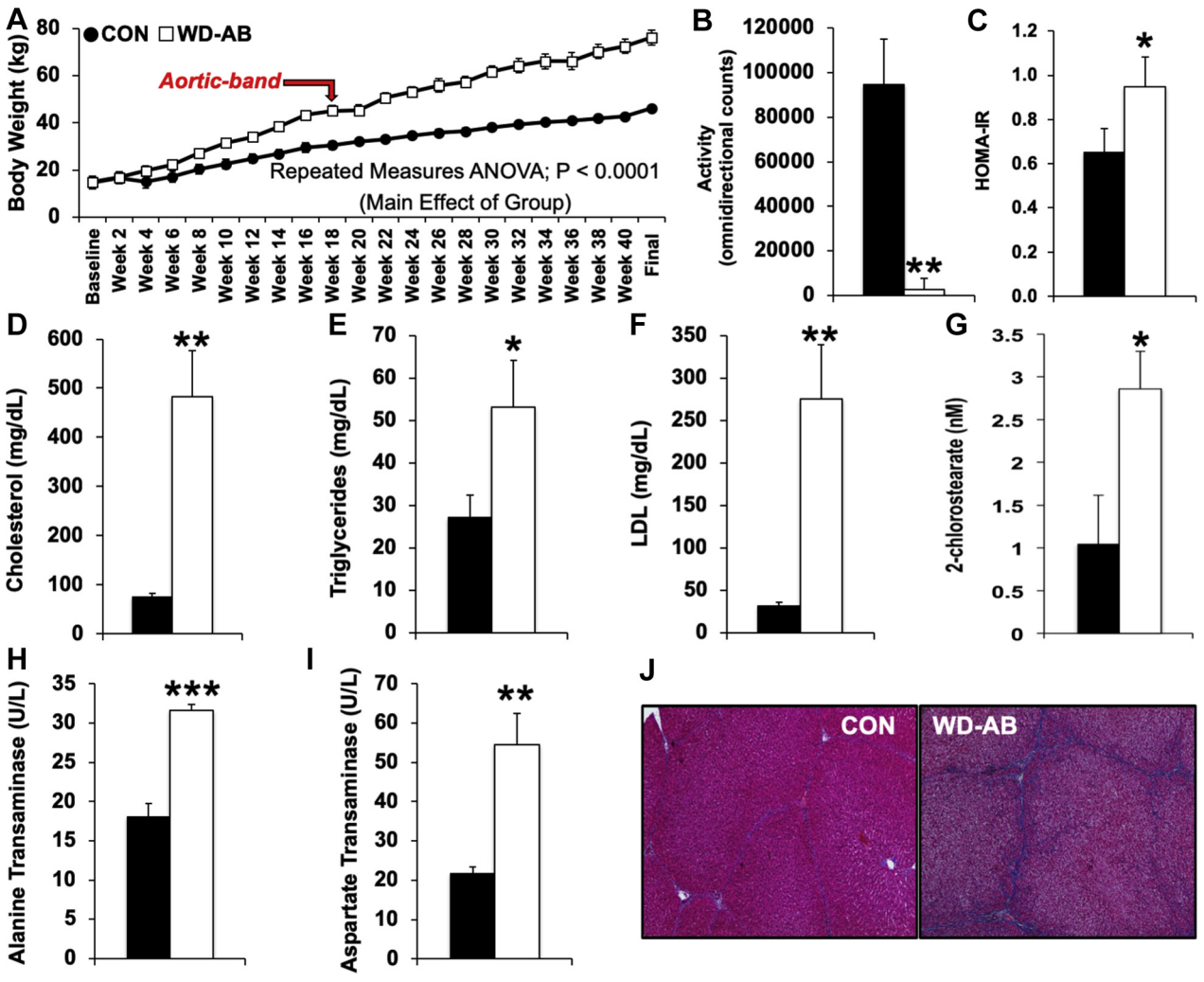

Animals in the WD-AB group were **(A)** obese, **(B)** inactive, and **(C)** insulin resistant (homeostatic model assessment of insulin resistance [HOMA-IR]). Dyslipidemia was observed in WD-AB animals as indicated by **(D)** increased plasma cholesterol, **(E)** triglycerides, **(F)** low-density lipoproteins (LDL), and **(G)** 2-chlorostearate. **(H and I)** Plasma liver enzymes were increased and evidence of (**J**; Masson's trichrome stain) increased liver fibrosis were seen in the WD-AB group. *t-test versus CON (*$p < 0.05$; **$p < 0.01$; ***$p < 0.001$). n = 5 for CON and WD. Abbreviations as in Figures 1 and 2.

that molecular mechanisms potentially relevant to HF are present in this model.

PERIPHERAL AND CENTRAL VASCULAR FUNCTION. Microvascular dysfunction, reflected by impaired vasodilatory capacity, was present in the skeletal muscle, brain, and coronary resistance vessels of WD-AB animals. Figure 5 shows conduit and resistance vessel function from the skeletal muscle and brain following exposure to endothelial (acetylcholine, bradykinin, insulin) and smooth muscle–dependent (sodium nitroprusside) vasodilators. Although conduit vessel function from both peripheral vascular beds was similar to the brachial artery (Figures 5A and 5B) and the carotid artery (Figures 5F and 5G) in the CON group, endothelial, metabolic, and smooth muscle–mediated vasodilatory capacity was impaired in the resistance arteries from isolated skeletal muscle (Figures 5C to 5E) and brain (Figures 5H to 5J) arterioles in the WD-AB group (complete dose–response curves for resistance vessels are shown in Supplemental Figures 4 to 5). In addition, in vivo evaluation of coronary vascular function demonstrated that although relative coronary blood flow was similar between groups (Supplemental Figure 6A, measured in the left

anterior descending coronary artery), myocardial oxygen extraction was greater in the WD-AB group (Supplemental Figure 6B). This was associated with impaired coronary resistance vessel vasodilatory capacity to the large conductance calcium-activated potassium (BKCa) channel agonist NS-1619 in isolated arterioles (Supplemental Figures 6C and 6D, a mediator of arterial tone abundantly expressed in vascular smooth muscle shown to provide protection against excessive vasoconstriction) (24,52-54). Gene ontology analysis revealed significant enrichment of several molecular pathways related to vascular disease, including atherosclerosis, microvascular complications, and peripheral vascular disease (Supplemental Table 2). In summary, these data indicate endothelial, metabolic, and smooth muscle–dependent microvascular dysfunction dominate vascular impairment in both the periphery and heart of WD-AB animals, which is consistent with functional vascular abnormalities seen in both cardio-metabolic disease and HF.

COMORBIDITIES AND INFLAMMATION. Before aortic banding, the body weight of WD-AB animals was significantly increased compared with CON, which indicated metabolic disease was developing at the time of surgery. The data presented in **Figures 6A to 6J and Table 2** show evidence of metabolic derangement at the time terminal experiments were performed. Specifically, obesity (body weight) (**Figures 6A, Table 2**), inactivity (decreased animal movement in the pen) (**Figure 6B**), insulin resistance (homeostatic model assessment of insulin resistance) (**Figure 6C**), and plasma hyperlipidemia (**Figures 6D to 6G**) (including chlorinated lipids [**Figure 6G**] associated with increased immune-derived reactive oxygen species production, inflammatory signaling, and endothelial dysfunction) (55-58) were seen in the WD-AB group. Wound healing in the WD-AB group following surgical intervention was excellent, and all animals were ambulatory, eating, urinating, and defecating normally within 1 week post-surgery. Thus, the significant decrease in cage activity in WD-AB animals was not related to our surgical procedures or other health concerns separate from the aortic banding or dietary interventions. Increased plasma liver enzyme levels and nonalcoholic fatty liver disease (**Figures 6H to 6J**) (evident by the combination of liver steatosis, inflammation, and fibrosis) in WD-AB animals was also consistent with nonalcoholic steatohepatitis as shown previously in WD-fed Ossabaw swine by our laboratory (14). Several reports indicate nonalcoholic steatohepatitis is related to HF and LV diastolic dysfunction (59-63). Further exploration of group differences that examined metabolic and renal disease, including immune and inflammation-related signaling pathways and phenotypes, were assessed using RNA-seq in LV tissue and is presented in Supplemental Figures 7 and 8 and Supplemental Tables 1 to 3. Enhancement of molecular pathways related to obesity, metabolic syndrome, diabetes, fatty liver disease, glomerulonephritis, and renal fibrosis were revealed following gene ontology analysis (Supplemental Table 2). A number of corresponding signaling pathways (Supplemental Table 3) and genetic phenotypes (Supplemental Table 4) highlighted immune and inflammatory involvement. Three of the top 5 significant upstream regulators identified by ingenuity pathway analysis indicated activation of well-known signaling networks that contributed to systemic inflammation, including tumor necrosis factor (Supplemental Figure 7A) ($p < 0.05$), interferon-γ (Supplemental Figure 7B) ($p < 0.05$), and toll-like receptor 3 (Supplemental Figure 7C) ($p < 0.05$). Top regulator effect gene networks that support activation (Supplemental Figure 8A) ($p < 0.05$), migration (Supplemental Figure 8A, $p < 0.05$), and adhesion (Supplemental Figure 8B) ($p < 0.05$) of immune cells potentially influenced by NF-κB signaling pathways (Supplemental Table 3, Supplemental Figure 8B) (CHUK-inhibitor of NF-κB kinase subunit-α) were also identified. Together, these findings suggest this preclinical model displays a chronic inflammatory state consistent with cardio-metabolic disease and HF.

DISCUSSION

This multidisciplinary research study showed that Ossabaw swine fed a WD and subjected to chronic cardiac pressure-overload exhibited functional, structural, and genetic characteristics consistent with cardio-metabolic HF. In this experimental setting, WD-AB animals displayed a number of cardiac and vascular features reminiscent of metabolic derangement and HF, including comorbidities associated with activation of the immune system and inflammation. Collectively, these data indicated the combination of traditional methods used to generate HF (i.e., diet, aortic-banding) imposed on the unique genetic background of Ossabaw swine resulted in a translational animal model with a distinctive constellation of findings that are conceivably useful to extending the understanding of how pre-existing cardio-metabolic syndrome can contribute to developing HF.

As hypothesized, WD-AB animals displayed cardiac characteristics fundamental to HF, including traditional indicators, myocardial remodeling, diastolic

dysfunction, and signs of altered, but compensated resting systolic function. Conventional markers of HF were observed at both system and molecular levels as shown by post-mortem, imaging, and molecular signatures that highlighted pathological cardiac remodeling (increased diastolic wall thickness), pulmonary involvement, and classic HF-related genes (e.g., natriuretic peptides, myosin heavy chain). Diastolic dysfunction was evident at the whole heart level in the WD-AB group by both an increase in the EDPVR and mechanically via abnormal diastolic strain measures, which implied difficulty filling during early diastole, with attempts to compensate for this deficiency by increasing the contributions of atrial systole to overall LV filling (64-68). Increased EDPVR and altered LV diastolic mechanics, observed in parallel with increased aortic systolic pressure, pulse pressure, and directionally consistent (but nonsignificant) increases in mean arterial pressure, effective arterial elastance, end-systolic elastance, and a decreased effective arterial elastance/end-systolic elastance ratio are evocative of HFpEF (69). LV end-diastolic pressure may not be elevated in early HFpEF (70,71); thus, our findings outline a reasonable scenario in which both vascular and ventricular stiffening could lead to the increase in the wet lung weight observed in the WD-AB group in the present study. In addition, an impaired ability of cardiomyocytes to sequester calcium and relax during diastole following β-adrenergic agonism signified a decrease in cellular diastolic cardiac reserve. Molecular signatures also indicated detrimental LV remodeling, as verified by evidence of collagen and titin isoform shifts, could increase the stiffness of the myocardium in parallel with LV mitochondrial dysfunction (via associated deficits in energetic need impairing excitation–contraction coupling).

Although compensated at rest, physiological assessment of systolic function indicated a number of paradoxical findings in the whole organ and a lack of cardiac reserve in isolated cardiomyocytes from the WD-AB group. A specific example of this inconsistency included no group differences in what would be considered a normal EF (>50%), observed in parallel with increased LV contractility (preload recruitable stroke work) and reduced systemic perfusion as indicated by the decreased stroke volume index. This contradiction also existed at the cellular level in WD-AB animals, as individual cardiomyocytes displayed normal absolute calcium transient and shortening amplitude, yet had an associated reduction in kinetic reserve capacity in response to adrenergic challenge with dobutamine. Such findings were consistent with those in rodent models of hypertrophy, in which cardiomyocyte functional parameters are maintained or enhanced (72,73), which may serve as an initial compensatory mechanism used by the heart to maintain systolic function at rest (74). However, such functional adaptations might consume a large portion of the cardiac reserve that normal healthy hearts typically maintain. This functional compensation, disguised at rest, becomes apparent during scenarios of increasing cardiovascular stress (e.g., activities of daily living, exercise), limiting the flexibility of the heart to respond to increasing hemodynamic demand. Together, this collection of data provides a solid foundation of evidence supporting the presence of experimental HF in WD-AB animals.

Increasing evidence suggests peripheral vascular dysfunction also plays a significant role in the lack of cardiovascular reserve and high prevalence of cardiogenic dementia in patients with HF. Our results indicate that at this stage of disease, a profile of primarily microvascular dysfunction reminiscent of HFpEF was observed in this translational model, as opposed to impaired conduit artery function which is more often associated with HFrEF (75-87). Novel data from the WD-AB group indicated there was a significant smooth muscle component to this profile of functional microvascular impairment in multiple vascular beds, including those supplying skeletal muscle, the brain, and the heart. Vascular mechanisms targeting smooth muscle may have therapeutic value given smooth muscle-mediated vascular dysfunction has been observed in resistance vessels from both the heart and the brain of Ossabaw swine with metabolic syndrome that did not have HF (88), and aortic-banded Yucatan mini-swine that displayed HF in the absence of metabolic comorbidities (24,26). A good deal of focus has also been placed on endothelial impairment caused by chronic inflammation as a driving force behind the development of cardiometabolic syndrome and HF. Our results likewise showed both endothelial and metabolic microvascular dysfunction in WD-AB animals (again in multiple vascular beds). A potential intersection between smooth muscle and endothelial-dependent vascular dysfunction could be nitric oxide, manifested via impaired downstream cGMP/PKG signaling that could negatively affect LV function from both a vascular and myocardial perspective (44). Diminished microvascular function, regardless of cellular mechanism, could significantly impact a patient's ability to engage in normal activities of daily living via: 1) a limited ability to increase blood flow to skeletal muscle and/or the heart in response to increased metabolic demand; or 2) by harming cognitive function potentially

leading to depression, dementia, and reduced therapeutic compliance. Together, these data indicate vascular impairment in WD-AB animals is dominated by microvascular dysfunction in multiple organs. We provide new evidence of a significant smooth muscle–mediated component to the disease process, in addition to metabolic and endothelial-dependent impairment. These findings are consistent with paradigms believed to reflect a scenario of cardio-metabolic HF.

CLINICAL PERSPECTIVES. The combination of multisystem genetic signatures, considered in parallel with a profile of metabolic disease, including obesity, inactivity, and dyslipidemia, supports the initial decision to use Ossabaw swine for this study given their genetic predisposition to this cluster of health disparities. From a molecular perspective, mRNA transcriptome signatures from the LV support our pathophysiological evidence of experimental HF and extensive cardio-metabolic disease in the WD-AB group. The molecular changes are highlighted by genes and pathways that are also implicated in numerous cardiac, vascular, metabolic, renal, immune, and inflammation-related signaling pathways. In particular, bone morphogenic protein–related pathways and NF-κB–mediated inflammatory gene induction are stimulated by transforming growth factor-β, tumor necrosis factor-α, and interleukin-1 signaling (89-91). These pathways, in addition to IL1RL1 (also part of the IL-1 super family) (92,93), were observed in the hearts of WD-AB animals. Anti-inflammatory therapy, including interleukin-1 and transforming growth factor-β inhibition, could be tested in the preclinical cardio-metabolic HF model presented here and contribute to the continuing evaluation of these therapeutic targets, which are currently being examined in clinical trials for both HFrEF and HFpEF (94-97).

In addition, ingenuity pathway analysis revealed significant gene signatures associated with activation, migration, and adhesion of immune cells potentially regulated in part by Inhibitor of NFκB Kinase Subunit Alpha (CHUK), a component of the NFκB signaling complex that, counterintuitive to its title, prompts activation of NFκB signaling (90,91). Results from unbiased '-omics'-based analysis between groups indicate a strong role for NFκB signaling in WD-AB animals, which can be activated by chlorinated lipids such as 2-chlorostearate. Chlorinated lipids can be generated from myeloperoxidase, a protein expressed in neutrophils, monocytes, and leukocytes that has been linked to inflammation and endothelial dysfunction (55-57). Therapeutic modulation of diet, including manipulation of lipid intake, has been linked to diastolic function and cardiovascular risk in HFpEF patients (98-100). Our results suggest this animal model could be a suitable platform to examine nutritional interventions as a way to modulate the pathological inflammation and vascular dysfunction associated with cardio-metabolic HF.

Systemic inflammation is highly correlated with metabolic derangement, and our results also found several gene networks reflecting inflammatory and immune signaling pathways were induced in the WD-AB group, including well-established molecular targets such as tumor necrosis factor, interferon-γ, and toll-like receptor 3 (101-105). The finding of inflammatory markers, such as PTX3 and IL1RL1, may also have potential diagnostic importance (43-45). PTX3 has been correlated with diastolic dysfunction (106,107), and IL1RL1 is mechanistically linked to the regulation of myocardial fibrosis (104,105,108). Molecular validation of these targets in WD-AB animals, and the association of PTX3 and IL1RL1 with LV untwisting during early diastole, provides further support of potential links between their levels and impaired diastolic function. These relationships warrant further mechanistic interrogation.

Other molecular targets that recently garnered attention for their therapeutic potential to treat HF include phosphodiesterase-9 (109) and histone deacetylases such as HDAC9 (110). These mechanisms appear as genes of interest in the cardiac hypertrophy and fibrosis networks presented in **Figure 4A** that are significantly altered in this translational model of cardio-metabolic HF. Considered together, the results of this study reveal a number of cellular mechanisms potentially applicable to a cardio-metabolic phenotype characterized by diet and comorbidity-driven inflammation. Accordingly, these data provide numerous avenues of exploration that we believe could be tested in this new preclinical platform of cardio-metabolic HF.

STUDY LIMITATIONS. The assessment of cardiac reserve is powerful as a diagnostic tool for assessing HF. In the present study, we assessed cardiac reserve at only the cellular level. Our group has a history of using both exercise and dobutamine dose–response protocols in the catheter laboratory to assess cardiac reserve in vivo (22-25,27,111-113). Although practical considerations (including an extensive focus on the transcriptome) limited our ability to perform these experiments, examination of cardiac reserve in future studies will be important to the continued verification of HF in this model. A comprehensive examination of cardiomyocyte calcium fluxes was not

performed, and the functional changes in calcium handling proteins in this disease model remain to be determined. We anticipate these changes are multifactorial based on our findings, and suggest complex changes in expression and/or post-translational modification of multiple calcium handling proteins. The transcriptome results presented in this study only suggest that certain molecular signatures in the heart share the same profile as observed in other diseases (e.g., renal pathology). By itself, the renal RNA-seq data observed from LV samples was not sufficient to establish etiology or mechanism, and further interrogation of kidney disease and its relationship to developing HF is warranted. A strength of this model is the statistical justification of a strong pathological phenotype in the animals, despite the large variability inherent to disease. Nevertheless, more subtle phenotypes that could be of physiological importance may be difficult to resolve with the present study design, and follow-up studies will be essential to extend the clinical translation of our initial findings.

CONCLUSIONS

Our results indicate the combination of pressure-overload and dietary intervention results in a profile of cardio-metabolic HF in Ossabaw swine. This unique preclinical animal model provides the opportunity to enhance our understanding of how metabolic disease interacts with developing HF, as well as a translational opportunity to develop new mechanistic avenues of exploration relevant to pathological conditions when symptoms of both cardio-metabolic disease and HF are present.

ACKNOWLEDGMENTS The authors would like to thank Michelle Gastecki, Grace Meers, Michelle Lambert, Rory Cunningham, Matt Panasevich, and Madeleine Dionne for their considerable technical contributions, which were essential to the successful completion of the study, and Gore for their generous gift of vascular Gore-Tex sleeves used for aortic banding. This work was supported with resources and the use of facilities at the Harry S. Truman Memorial Veterans Hospital in Columbia, Missouri.

ADDRESS FOR CORRESPONDENCE: Dr. Craig A. Emter, Dr. R. Scott Rector, Dr. Jaume Padilla, and Dr. Timothy L. Domeier, University of Missouri-Columbia, 1600 East Rollins, Columbia, Missouri 65211. E-mail: emterc@missouri.edu OR RectorS@health.missouri.edu OR padillaja@missouri.edu OR domeiert@health.missouri.edu.

PERSPECTIVES

COMPETENCY IN MEDICAL KNOWLEDGE: The development of new treatments for HF has suffered from a lack of animal models that encompass the increasingly heterogeneous disease profile of this patient population. This report provides evidence supporting the hypothesis that WD-AB Ossabaw swine displayed an integrated physiological, morphological, and genetic phenotype evocative of cardio metabolic HF.

TRANSLATIONAL OUTLOOK: This new preclinical animal model displayed a distinctive constellation of findings that are conceivably useful to extending the understanding of how pre-existing cardio-metabolic syndrome can contribute to developing HF.

REFERENCES

1. Borlaug BA, Paulus WJ. Heart failure with preserved ejection fraction: pathophysiology, diagnosis, and treatment. Eur Heart J 2011;32:670–9.

2. Maeder MT, Kaye DM. Heart failure with normal left ventricular ejection fraction. J Am Coll Cardiol 2009;53:905–18.

3. Oktay AA, Rich JD, Shah SJ. The emerging epidemic of heart failure with preserved ejection fraction. Curr Heart Fail Rep 2013;10:401–10.

4. Zhao Z, Wang H, Jessup JA, Lindsey SH, Chappell MC, Groban L. Role of estrogen in diastolic dysfunction. Am J Physiol Heart Circ Physiol 2014;306:H628–40.

5. Sharma K, Kass DA. Heart failure with preserved ejection fraction: mechanisms, clinical features, and therapies. Circ Res 2014;115:79–96.

6. Paulus WJ, van Ballegoij JJ. Treatment of heart failure with normal ejection fraction: an inconvenient truth! J Am Coll Cardiol 2010;55:526–37.

7. Burkhoff D. Mortality in heart failure with preserved ejection fraction: an unacceptably high rate. Eur Heart J 2012;33:1718–20.

8. Borlaug BA, Redfield MM. Diastolic and systolic heart failure are distinct phenotypes within the heart failure spectrum. Circulation 2011;123:2006–13. discussion 2014.

9. Zile MR, Kjellstrom B, Bennett T, et al. Effects of exercise on left ventricular systolic and diastolic properties in patients with heart failure and a preserved ejection fraction versus heart failure and a reduced ejection fraction. Circ Heart Fail 2013;6:508–16.

10. Bratz IN, Dick GM, Tune JD, et al. Impaired capsaicin-induced relaxation of coronary arteries in a porcine model of the metabolic syndrome. Am J Physiol Heart Circ Physiol 2008;294:H2489–96.

11. Dyson MC, Alloosh M, Vuchetich JP, Mokelke EA, Sturek M. Components of metabolic syndrome and coronary artery disease in female Ossabaw swine fed excess atherogenic diet. Comp Med 2006;56:35–45.

12. Neeb ZP, Edwards JM, Alloosh M, Long X, Mokelke EA, Sturek M. Metabolic syndrome and coronary artery disease in Ossabaw compared with Yucatan swine. Comp Med 2010;60:300–15.

13. Padilla J, Jenkins NT, Lee S, et al. Vascular transcriptional alterations produced by juvenile obesity in Ossabaw swine. Physiol Genomics 2013;45:434–46.

14. Panasevich MR, Meers GM, Linden MA, et al. High-fat, high-fructose, high-cholesterol feeding causes severe NASH and cecal microbiota dysbiosis in juvenile Ossabaw swine. Am J Physiol Endocrinol Metab 2018;314:E78–92.

15. Toedebusch RG, Roberts MD, Wells KD, et al. Unique transcriptomic signature of omental adipose tissue in Ossabaw swine: a model of childhood obesity. Physiol Genomics 2014;46:362–75.

16. Vieira-Potter VJ, Lee S, Bayless DS, et al. Disconnect between adipose tissue inflammation and cardiometabolic dysfunction in Ossabaw pigs. Obesity (Silver Spring) 2015;23:2421–9.

17. Olver TD, Grunewald ZI, Jurrissen TJ, et al. Microvascular insulin resistance in skeletal muscle and brain occurs early in the development of juvenile obesity in pigs. Am J Physiol Regul Integr Comp Physiol 2018;314:R252–64.

18. Fleenor BS, Ouyang A, Olver TD, et al. Saxagliptin prevents increased coronary vascular stiffness in aortic-banded mini swine. Hypertension 2018;72:466–75.

19. Hiemstra JA, Gutierrez-Aguilar M, Marshall KD, et al. A new twist on an old idea part 2: cyclosporine preserves normal mitochondrial but not cardiomyocyte function in mini-swine with compensated heart failure. Physiol Rep 2014;2:e12050.

20. Hiemstra JA, Lee DI, Chakir K, et al. Saxagliptin and tadalafil differentially alter cyclic guanosine monophosphate (cGMP) signaling and left ventricular function in aortic-banded mini-swine. J Am Heart Assoc 2016;5:e003277.

21. Hiemstra JA, Liu S, Ahlman MA, et al. A new twist on an old idea: a two-dimensional speckle tracking assessment of cyclosporine as a therapeutic alternative for heart failure with preserved ejection fraction. Physiol Rep 2013;1:e00174.

22. Hiemstra JA, Veteto AB, Lambert MD, et al. Chronic low-intensity exercise attenuates cardiomyocyte contractile dysfunction and impaired adrenergic responsiveness in aortic-banded miniswine. J Appl Physiol (1985) 2018;124:1034–44.

23. Marshall KD, Muller BN, Krenz M, et al. Heart failure with preserved ejection fraction: chronic low-intensity interval exercise training preserves myocardial O2 balance and diastolic function. J Appl Physiol (1985) 2013;114:131–47.

24. Olver TD, Edwards JC, Ferguson BS, et al. Chronic interval exercise training prevents BKCa channel-mediated coronary vascular dysfunction in aortic-banded miniswine. J Appl Physiol (1985) 2018;125:86–96.

25. Olver TD, Hiemstra JA, Edwards JC, Ferguson BS, Laughlin MH, Emter CA. The protective role of sex hormones in females and exercise prehabilitation in males on sternotomy-induced cranial hypoperfusion in aortic banded mini-swine. J Appl Physiol (1985) 2017;122:423–9.

26. Olver TD, Hiemstra JA, Edwards JC, et al. Loss of female sex hormones exacerbates cerebrovascular and cognitive dysfunction in aortic banded miniswine through a neuropeptide Y-Ca(2+)-activated potassium channel-nitric oxide mediated mechanism. J Am Heart Assoc 2017;6.

27. Olver TD, Klakotskaia D, Ferguson BS, et al. Carotid artery vascular mechanics serve as biomarkers of cognitive dysfunction in aortic-banded miniature swine that can be treated with an exercise intervention. J Am Heart Assoc 2016;5.

28. Douglas WR. Of pigs and men and research: a review of appreciation, and the logic of the pig in human medical research. Space Life Sci 1977;3:226–34.

29. Laughlin MH, Overholser KA, Bhatte MJ. Exercise training increases coronary transport reserve in miniature swine. J Appl Physiol (1985) 1989;67:1140–9.

30. Hurnik JF, Lewis NJ. Use of body surface area to set minimum space allowances for confined pigs and cattle. Can J Animal Sc 1991;71:577–80.

31. Esmay ML. Principles of animal environment. Westport, CT: AVI Publishing Co., Inc., 1978.

32. de Winter JCF. Using the Student's t-test with extremely small sample sizes. Pract Assess Res Eval 2013;18:1–12.

33. Tee MW, Won S, Raman FS, et al. Regional strain analysis with multidetector CT in a swine cardiomyopathy model: relationship to cardiac MR tagging and myocardial fibrosis. Radiology 2015;277:88–94.

34. Kim J, Seo BS. How to calculate sample size and why. Clin Orthoped Surg 2013;5:235–42.

35. Curran-Everett D, Benos DJ. Guidelines for reporting statistics in journals published by the American Physiological Society. Am J Physiol Regul Integr Comp Physiol 2004;287:R247–9.

36. Williams JL, Hathaway CA, Kloster KL, Layne BH. Low power, type II errors, and other statistical problems in recent cardiovascular research. Am J Physiol 1997;273:H487–93.

37. Yin FC, Spurgeon HA, Rakusan K, Weisfeldt ML, Lakatta EG. Use of tibial length to quantify cardiac hypertrophy: application in the aging rat. Am J Physiol 1982;243:H941–7.

38. Chirinos JA, Segers P, De Buyzere ML, et al. Left ventricular mass: allometric scaling, normative values, effect of obesity, and prognostic performance. Hypertension 2010;56:91–8.

39. Litwin SE. Cardiac "morphomics": do we need to measure LV mass and geometry in everyone? J Am Coll Cardiol Img 2015;8:1016–8.

40. Ishikawa K, Aguero J, Oh JG, et al. Increased stiffness is the major early abnormality in a pig model of severe aortic stenosis and predisposes to congestive heart failure in the absence of systolic dysfunction. J Am Heart Assoc 2015;4:e001925.

41. Sparagna GC, Chicco AJ, Murphy RC, et al. Loss of cardiac tetralinoleoyl cardiolipin in human and experimental heart failure. J Lipid Res 2007;48:1559–70.

42. Ventura-Clapier R, Garnier A, Veksler V. Energy metabolism in heart failure. J Physiol 2004;555:1–13.

43. Inoue K, Kodama T, Daida H. Pentraxin 3: a novel biomarker for inflammatory cardiovascular disease. Int J Vasc Med 2012;2012:657025.

44. Greene SJ, Gheorghiade M, Borlaug BA, et al. The cGMP signaling pathway as a therapeutic target in heart failure with preserved ejection fraction. J Am Heart Assoc 2013;2:e000536.

45. Shah SJ, Kitzman DW, Borlaug BA, et al. Phenotype-specific treatment of heart failure with preserved ejection fraction: a multiorgan roadmap. Circulation 2016;134:73–90.

46. Burgess ML, Buggy J, Price RL, et al. Exercise- and hypertension-induced collagen changes are related to left ventricular function in rat hearts. Am J Physiol 1996;270:H151–9.

47. Hidalgo C, Granzier H. Tuning the molecular giant titin through phosphorylation: role in health and disease. Trends Cardiovasc Med 2013;23:165–71.

48. Linke WA, Hamdani N. Gigantic business: titin properties and function through thick and thin. Circ Res 2014;114:1052–68.

49. Franssen C, Gonzalez Miqueo A. The role of titin and extracellular matrix remodelling in heart failure with preserved ejection fraction. Neth Heart J 2016;24:259–67.

50. Lewis GA, Schelbert EB, Williams SG, et al. Biological phenotypes of heart failure with preserved ejection fraction. J Am Coll Cardiol 2017;70:2186–200.

51. van Heerebeek L, Franssen CP, Hamdani N, Verheugt FW, Somsen GA, Paulus WJ. Molecular and cellular basis for diastolic dysfunction. Curr Heart Fail Rep 2012;9:293–302.

52. Berkefeld H, Fakler B, Schulte U. Ca2+-activated K+ channels: from protein complexes to function. Physiol Rev 2010;90:1437–59.

53. Hill MA, Yang Y, Ella SR, Davis MJ, Braun AP. Large conductance, Ca2+-activated K+ channels (BKCa) and arteriolar myogenic signaling. FEBS Lett 2010;584:2033–42.

54. Rusch NJ. BK channels in cardiovascular disease: a complex story of channel dysregulation. Am J Physiol Heart Circ Physiol 2009;297:H1580–2.

55. Ford DA. Lipid oxidation by hypochlorous acid: chlorinated lipids in atherosclerosis and myocardial ischemia. Clin Lipidol 2010;5:835–52.

56. Hartman CL, Duerr MA, Albert CJ, Neumann WL, McHowat J, Ford DA. 2-Chlorofatty acids induce Weibel-Palade body mobilization. J Lipid Res 2018;59:113–22.

57. Messner MC, Albert CJ, Ford DA. 2-Chlorohexadecanal and 2-chlorohexadecanoic acid induce COX-2 expression in human coronary artery endothelial cells. Lipids 2008;43:581–8.

58. Wang WY, Albert CJ, Ford DA. Alpha-chlorofatty acid accumulates in activated monocytes and causes apoptosis through reactive oxygen species production and endoplasmic reticulum stress. Arterioscler Thromb Vasc Biol 2014;34:526–32.

59. Chung GE, Lee JH, Lee H, et al. Nonalcoholic fatty liver disease and advanced fibrosis are associated with left ventricular diastolic dysfunction. Atherosclerosis 2018;272:137–44.

60. Mantovani A, Pernigo M, Bergamini C, et al. Nonalcoholic fatty liver disease is independently associated with early left ventricular diastolic dysfunction in patients with type 2 diabetes. PLoS One 2015;10:e0135329.

61. Simon TG, Bamira DG, Chung RT, Weiner RB, Corey KE. Nonalcoholic steatohepatitis is associated with cardiac remodeling and dysfunction. Obesity (Silver Spring) 2017;25:1313–6.

62. Takahashi T, Watanabe T, Shishido T, et al. The impact of non-alcoholic fatty liver disease fibrosis score on cardiac prognosis in patients with chronic heart failure. Heart Vessels 2018;33:733–9.

63. Yoshihisa A, Sato Y, Yokokawa T, et al. Liver fibrosis score predicts mortality in heart failure patients with preserved ejection fraction. ESC Heart Fail 2018;5:262–70.

64. Kosmala W, Plaksej R, Strotmann JM, et al. Progression of left ventricular functional abnormalities in hypertensive patients with heart failure: an ultrasonic two-dimensional speckle tracking study. J Am Soc Echocardiogr 2008;21:1309–17.

65. Park SJ, Miyazaki C, Bruce CJ, Ommen S, Miller FA, Oh JK. Left ventricular torsion by two-dimensional speckle tracking echocardiography in patients with diastolic dysfunction and normal ejection fraction. J Am Soc Echocardiogr 2008;21:1129–37.

66. Takeuchi M, Borden WB, Nakai H, et al. Reduced and delayed untwisting of the left ventricle in patients with hypertension and left ventricular hypertrophy: a study using two-dimensional speckle tracking imaging. Eur Heart J 2007;28:2756–62.

67. Morris DA, Boldt LH, Eichstadt H, Ozcelik C, Haverkamp W. Myocardial systolic and diastolic performance derived by 2-dimensional speckle tracking echocardiography in heart failure with normal left ventricular ejection fraction. Circ Heart Fail 2012;5:610–20.

68. Tan YT, Wenzelburger F, Lee E, et al. The pathophysiology of heart failure with normal ejection fraction: exercise echocardiography reveals complex abnormalities of both systolic and diastolic ventricular function involving torsion, untwist, and longitudinal motion. J Am Coll Cardiol 2009;54:36–46.

69. Borlaug BA, Kass DA. Ventricular-vascular interaction in heart failure. Heart Fail Clin 2008;4:23–36.

70. Andersen MJ, Borlaug BA. Invasive hemodynamic characterization of heart failure with preserved ejection fraction. Heart Fail Clin 2014;10:435–44.

71. Borlaug BA, Nishimura RA, Sorajja P, Lam CS, Redfield MM. Exercise hemodynamics enhance diagnosis of early heart failure with preserved ejection fraction. Circ Heart Fail 2010;3:588–95.

72. Curl CL, Danes VR, Bell JR, et al. Cardiomyocyte functional etiology in heart failure with preserved ejection fraction is distinctive-a new preclinical model. J Am Heart Assoc 2018;7.

73. Primessnig U, Schonleitner P, Holl A, et al. Novel pathomechanisms of cardiomyocyte dysfunction in a model of heart failure with preserved ejection fraction. Eur J Heart Fail 2016;18:987–97.

74. Peana D, Domeier TL. Cardiomyocyte Ca(2+) homeostasis as a therapeutic target in heart failure with reduced and preserved ejection fraction. Curr Opin Pharmacol 2017;33:17–26.

75. Lee JF, Barrett-O'Keefe Z, Garten RS, et al. Evidence of microvascular dysfunction in heart failure with preserved ejection fraction. Heart 2016;102:278–84.

76. Lee JF, Barrett-O'Keefe Z, Nelson AD, et al. Impaired skeletal muscle vasodilation during exercise in heart failure with preserved ejection fraction. Int J Cardiol 2016;211:14–21.

77. Borlaug BA, Olson TP, Lam CS, et al. Global cardiovascular reserve dysfunction in heart failure with preserved ejection fraction. J Am Coll Cardiol 2010;56:845–54.

78. Dhakal BP, Malhotra R, Murphy RM, et al. Mechanisms of exercise intolerance in heart failure with preserved ejection fraction: the role of abnormal peripheral oxygen extraction. Circ Heart Fail 2015;8:286–94.

79. Haykowsky MJ, Herrington DM, Brubaker PH, Morgan TM, Hundley WG, Kitzman DW. Relationship of flow-mediated arterial dilation and exercise capacity in older patients with heart failure and preserved ejection fraction. J Gerontol A Biol Sci Med Sci 2013;68:161–7.

80. Hundley WG, Bayram E, Hamilton CA, et al. Leg flow-mediated arterial dilation in elderly patients with heart failure and normal left ventricular ejection fraction. Am J Physiol Heart Circ Physiol 2007;292:H1427–34.

81. Athilingam P, D'Aoust RF, Miller L, Chen L. Cognitive profile in persons with systolic and diastolic heart failure. Congest Heart Fail 2013;19:44–50.

82. Cermakova P, Lund LH, Fereshtehnejad SM, et al. Heart failure and dementia: survival in relation to types of heart failure and different dementia disorders. Eur J Heart Fail 2015;17:612–9.

83. Dodson JA, Truong TT, Towle VR, Kerins G, Chaudhry SI. Cognitive impairment in older adults with heart failure: prevalence, documentation, and impact on outcomes. Am J Med 2013;126:120–6.

84. van den Hurk K, Reijmer YD, van den Berg E, et al. Heart failure and cognitive function in the general population: the Hoorn Study. Eur J Heart Fail 2011;13:1362–9.

85. Haykowsky MJ, Brubaker PH, John JM, Stewart KP, Morgan TM, Kitzman DW. Determinants of exercise intolerance in elderly heart failure patients with preserved ejection fraction. J Am Coll Cardiol 2011;58:265–74.

86. Upadhya B, Haykowsky MJ, Eggebeen J, Kitzman DW. Exercise intolerance in heart failure with preserved ejection fraction: more than a heart problem. J Geriatr Cardiol 2015;12:294–304.

87. Dryer K, Gajjar M, Narang N, et al. Coronary microvascular dysfunction in patients with heart failure with preserved ejection fraction. Am J Physiol Heart Circ Physiol 2018;314:H1033–42.

88. Borbouse L, Dick GM, Asano S, et al. Impaired function of coronary BK(Ca) channels in metabolic syndrome. Am J Physiol Heart Circ Physiol 2009;297:H1629–37.

89. Guo X, Wang XF. Signaling cross-talk between TGF-beta/BMP and other pathways. Cell Res 2009;19:71–88.

90. Hayden MS, Ghosh S. Shared principles in NF-kappaB signaling. Cell 2008;132:344–62.

91. Solt LA, May MJ. The IkappaB kinase complex: master regulator of NF-kappaB signaling. Immunol Res 2008;42:3–18.

92. Griesenauer B, Paczesny S. The ST2/IL-33 axis in immune cells during inflammatory diseases. Front Immunol 2017;8:475.

93. Sanada S, Hakuno D, Higgins LJ, Schreiter ER, McKenzie AN, Lee RT. IL-33 and ST2 comprise a critical biomechanically induced and cardioprotective signaling system. J Clin Invest 2007;117:1538–49.

94. AbouEzzeddine OF, McKie PM, Dunlay SM, et al. Suppression of tumorigenicity 2 in heart failure with preserved ejection fraction. J Am Heart Assoc 2017;6.

95. Hartman MHT, Groot HE, Leach IM, Karper JC, van der Harst P. Translational overview of cytokine inhibition in acute myocardial infarction and chronic heart failure. Trends Cardiovasc Med 2018;28:369–79.

96. McCarthy CP, Januzzi JL Jr. Soluble ST2 in heart failure. Heart Fail Clin 2018;14:41–8.

97. Panahi M, Papanikolaou A, Torabi A, et al. Immunomodulatory interventions in myocardial infarction and heart failure: a systematic review of clinical trials and meta-analysis of IL-1 inhibition. Cardiovasc Res 2018;114:1445–61.

98. Carbone S, Canada JM, Buckley LF, et al. Dietary fat, sugar consumption, and cardiorespiratory fitness in patients with heart failure with preserved ejection fraction. J Am Coll Cardiol Basic Transl Sci 2017;2:513–25.

99. Tschope C, Birner C, Bohm M, et al. Heart failure with preserved ejection fraction: current management and future strategies: expert opinion on the behalf of the Nucleus of the "Heart Failure Working Group" of the German Society of Cardiology (DKG). Clin Res Cardiol 2018;107:1–19.

100. von Bibra H, Strohle A, St John Sutton M, Worm N. Dietary therapy in heart failure with preserved ejection fraction and/or left ventricular diastolic dysfunction in patients with metabolic syndrome. Int J Cardiol 2017;234:7–15.

101. Asghar A, Sheikh N. Role of immune cells in obesity induced low grade inflammation and insulin resistance. Cell Immunol 2017;315:18–26.

102. Lauterbach MA, Wunderlich FT. Macrophage function in obesity-induced inflammation and insulin resistance. Pflugers Arch 2017;469:385–96.

103. Saltiel AR, Olefsky JM. Inflammatory mechanisms linking obesity and metabolic disease. J Clin Invest 2017;127:1–4.

104. D'Elia E, Vaduganathan M, Gori M, Gavazzi A, Butler J, Senni M. Role of biomarkers in cardiac structure phenotyping in heart failure with

preserved ejection fraction: critical appraisal and practical use. Eur J Heart Fail 2015;17:1231–9.

105. Meijers WC, van der Velde AR, de Boer RA. Biomarkers in heart failure with preserved ejection fraction. Neth Heart J 2016;24:252–8.

106. Abernethy A, Raza S, Sun JL, et al. Pro-Inflammatory biomarkers in sTable versus acutely decompensated heart failure with preserved ejection fraction. J Am Heart Assoc 2018;7.

107. Matsubara J, Sugiyama S, Nozaki T, et al. Pentraxin 3 is a new inflammatory marker correlated with left ventricular diastolic dysfunction and heart failure with normal ejection fraction. J Am Coll Cardiol 2011;57:861–9.

108. Sanders-van Wijk S, van Empel V, Davarzani N, et al. Circulating biomarkers of distinct pathophysiological pathways in heart failure with preserved vs. reduced left ventricular ejection fraction. Eur J Heart Fail 2015;17:1006–14.

109. Lee DI, Zhu G, Sasaki T, et al. Phosphodiesterase 9A controls nitric-oxide-independent cGMP and hypertrophic heart disease. Nature 2015;519:472–6.

110. Jeong MY, Lin YH, Wennersten SA, et al. Histone deacetylase activity governs diastolic dysfunction through a nongenomic mechanism. Sci Transl Med 2018;10.

111. Emter CA, Baines CP. Low-intensity aerobic interval training attenuates pathological left ventricular remodeling and mitochondrial dysfunction in aortic-banded miniature swine. Am J Physiol Heart Circ Physiol 2010;299:H1348–56.

112. Emter CA, Tharp DL, Ivey JR, Ganjam VK, Bowles DK. Low-intensity interval exercise training attenuates coronary vascular dysfunction and preserves Ca(2)(+)-sensitive K(+) current in miniature swine with LV hypertrophy. Am J Physiol Heart Circ Physiol 2011;301:H1687–94.

113. McDonald KS, Emter CA. Exploring new concepts in the management of heart failure with preserved ejection fraction: is exercise the key for improving treatment? J Appl Physiol (1985) 2015;119:724–5.

KEY WORDS cardio-metabolic disease, heart failure, integrative pathophysiology, preclinical model of cardiovascular disease

APPENDIX For an expanded Methods section and supplemental figures and tables, please see the online version of this paper.